Title: Crystallization of Fe72B20Si4Nb4 metallic glasses ribbons

Author: Ryszard Nowosielski, Rafał Babilas, Stefan Griner, Grzegorz Dercz, Aneta Hanc

Citation style: Nowosielski Ryszard, Babilas Rafał, Griner Stefan, Dercz Grzegorz, Hanc Aneta. (2009). Crystallization of Fe72B20Si4Nb4 metallic glasses ribbons. "Journal of Achievements in Materials and Manufacturing Engineering" (Vol. 34, iss. 1 (2009), s. 15-22).

Journal of Achievements in Materials and Manufacturing Engineering
VOLUME 34
ISSUE 1
May
2009

Crystallization of $Fe_{72}B_{20}Si_4Nb_4$ metallic glasses ribbons

R. Nowosielski [a], R. Babilas [a,*], S. Griner [a], G. Dercz [b], A. Hanc [b]
[a] Division of Nanocrystalline and Functional Materials and Sustainable Pro-ecological Technologies, Institute of Engineering Materials and Biomaterials, Silesian University of Technology, ul. Konarskiego 18a, 44-100 Gliwice, Poland
[b] Institute of Materials Science, University of Silesia, ul. Bankowa 12, 40-007 Katowice, Poland
* Corresponding author: E-mail address: rafal.babilas@polsl.pl

Received 12.02.2009; published in revised form 01.05.2009

Materials

ABSTRACT

Purpose: The paper presents a crystallization process of Fe-based amorphous materials. The aim of work is presentation of the influence of annealing temperature on structural changes and magnetic properties of $Fe_{72}B_{20}Si_4Nb_4$ metallic glasses.
Design/methodology/approach: The studies were performed on metallic glasses as ribbons. Crystallization behaviour of the studied alloy was examined by differential thermal analysis (DTA), X-ray diffraction (XRD), transmission electron microscopy (TEM) and Mössbauer spectroscopy methods. The soft magnetic properties examination of tested material contained magnetic permeability, coercive field, saturation induction and magnetic after-effects measurements.
Findings: The XRD, TEM and Mössbauer spectroscopy investigations revealed that the studied alloy in as-cast state was amorphous. A two stage crystallization process was observed for studied material. The first stage of crystallization corresponding to the partial crystallization of α-Fe phase was followed by the formation of iron borides. It has shown that appropriate increasing of annealing temperature, significantly improved soft magnetic properties of examined alloy. The maximum of initial magnetic permeability is correlated with a minimum of coercive field.
Practical implications: The soft magnetic properties of metallic glasses can be optimized by applying the appropriate conditions of heat treatment.
Originality/value: The applied investigation methods are suitable to determine the changes of structure and the improvement of soft magnetic properties of examined Fe-based alloy in comparison with as-cast state.
Keywords: Amorphous materials; Structural relaxation; Crystallization; Soft magnetic properties

Reference to this paper should be given in the following way:
R. Nowosielski, R. Babilas, S. Griner, G. Dercz, A. Hanc, Crystallization of $Fe_{72}B_{20}Si_4Nb_4$ metallic glasses ribbons, Journal of Achievements in Materials and Manufacturing Engineering 34/1 (2009) 15-22.

1. Introduction

Multicomponent Fe-based amorphous alloys have a lot of attention due to their good soft magnetic properties combined with high glass-forming ability. These features enable to produce soft ferromagnetic materials in bulk amorphous forms of ribbons, rods, rings or plates [1-3].

Thermal stability and glass-forming behaviour of the iron-based bulk amorphous alloys have been studied widely. It is

generally known that amorphous alloys tend to thermodynamic equilibrium by two ways: structural relaxation and crystallization process. Structural relaxation of amorphous materials leads to changes in their physical properties. These changes are due to atomic rearrangements that lead to changes in free volume [4].

Soft magnetic properties of Fe-based ferromagnetic amorphous alloys could be significantly improved by a controlling heat treatment (crystallization process) [2].

The investigation of the crystallization process is important for understanding the mechanisms of phase transformation from equilibrium, the thermal stability of metallic glasses and for producing controlled microstructures. Since the formation of metallic glasses was getting easier, much work has been devoted to their crystallization. However, a proper understanding for the thermal stability against crystallization of the metallic glasses is still lacking [5].

Crystallization under various conditions could be precisely investigated by many methods like differential scanning calorimetry (DSC), differential thermal analysis (DTA), X-ray diffraction (XRD), neutron scattering, density and acoustic measurements. That studies could also provide information for understanding the influence of microstructure changes on physical properties during relaxation, nanocrystallization and crystallization processes [1,5].

In general, the scheme of crystallization process of metallic glasses is following. At the initial stage of crystallization process, there are formed metallic elements and their solutions. When the process is more advanced, there are formed borides of metal and intermetallic phases. Table 1 presents examples of crystallization's products of chosen Fe-based metallic glasses [2].

Table 1.
Products of crystallization process of chosen metallic glasses [1,2]

Glassy alloy	Products of crystallization process
$Fe_{75}Si_{15}B_{10}$	αFe(Si), Fe_3B, Fe_2B, Fe_3Si
$Fe_{77.5}Si_{13.5}B_9$	αFe(Si), Fe_3B
$Fe_{70}Cr_{18}B_{10}Ti_2$	αFe, $(Fe,Cr)_3B$
$Fe_{81}Si_{13.5}B_{13.5}C_2$	αFe(Si,C), Fe_3B, Fe_2B
$Fe_{76.5}Cu_1Si_{13.5}B_9$	αFe(Si)
$Fe_{73.5}Cu_1Ta_3Si_{13.5}B_9$	αFe(Si), Fe_3Si
$Fe_{73.5}Cu_1Nb_3Si_{13.5}B_9$	αFe(Si), Fe_3Si
$Fe_{73.5}Si_{13.5}B_9Nb_3Cu_1$	αFe, Fe_3B, $Fe_{23}B_6$, Fe_2B
$Fe_{74.5}Nb_3Si_{13.5}B_9$	αFe(Si), Fe_3B
$Fe_{75}Co_3Si_9B_{13}$	αFe, $(Fe,Co)_3B$, $(Fe,Co)_2B$,
$Fe_{76}Cr_2Si_8B_{14}$	αFe(Si), Fe_3Si, Fe_3B, Fe_2B
$Fe_{76}Mo_2Si_8B_{14}$	αFe(Si), Fe_3Si, Fe_3B, FeMo
$Fe_{86}Zr_7Cu_1B_6$	αFe

Improving of magnetic properties (usually magnetic permeability) of metallic glasses is a result of formation a nanocrystalline phase. What is important, the enhancement of magnetic permeability is also could be explained by decrease of magnetostriction constant and annealing out of microvoids [2,3].

2. Material and research methodology

The aim of the this paper is the microstructure analysis and magnetic properties characterization of $Fe_{72}B_{20}Si_4Nb_4$ metallic glass samples after annealing process using XRD, TEM, Mössbauer spectroscopy, DTA, VSM and magnetic methods.

The investigated materials were cast as ribbon shaped metallic glasses with thickness 0.03 mm and width 10 mm. The ribbons were manufactured by the "chill-block melt spinning" (CBMS) technique, which is a method of continuous casting of the liquid alloy on the surface of a turning copper based wheel [6-10].

The casting conditions include linear speed of copper wheel: 20 m/s and ejection over-pressure of molten alloy: 200 mBar.

The chemical composition of studied Fe-based metallic glass allows to cast this kind of material in bulk forms, but in this work used samples in form of ribbons.

In order to study structural relaxation and crystallization processes samples in the "as-cast" state were annealed at the temperature range from 373 to 923 K with the step of 50 K. Tested ribbons were annealed in electric chamber furnace THERMOLYNE 6020C under protective argon atmosphere. The annealing time was constant and equaled to 1 hour.

Phase analysis was carried out using the X-Pert Philips diffractometer equipped with curved graphite monochromator on diffracted beam and a tube provided with copper anode [11]. It was supplied by current intensity of 30 mA and voltage of 40 kV. The length of radiation ($\lambda Cu_{K\alpha}$) was 1.54178 Å. The data of diffraction lines were recorded by "step-scanning" method in 2θ range from 30° to 90° and 0.05° step.

Transmission electron microscopy (TESLA BS 540) was used for the structural characterization of studied samples after annealing process. Thin foils for TEM observation were prepared by an electrolytic polishing method after a mechanical grinding.

The thermal properties associated with crystallization temperature of the amorphous ribbons and liquidus temperature of master alloy were measured using the differential thermal analysis (Mettler - DTA) at a constant heating rate of 6 K/s under an argon protective atmosphere.

Magnetic measurements of annealed samples (determined at room temperature) included following properties:
(1) relative magnetic permeability - determined by Maxwell-Wien bridge at a frequency of 1030 Hz and magnetic field H= 0.5 A/m), (magnetic permeability measurements were carried out for ribbons of length of 100 mm);
(2) coercive field - measured by coercivemeter (permalloy probe);
(3) magnetic permeability relaxation $\Delta\mu/\mu$ (magnetic after-effects) - determined by measuring changes of magnetic permeability as a function of time after demagnetization, where $\Delta\mu$ is difference between magnetic permeability determined at t_1 = 30 s and t_2 = 1800 s after demagnetization and μ at t_1 [12,13].

The magnetic hysteresis loops of studied metallic glasses were measured by the resonance vibrating sample magnetometer (R-VSM) presented by Wrona et al. [14]. R-VSM measurements deliver information about averaged magnetization process from the whole volume of the tested sample, which oscillates in parallel to the direction of external magnetic field.

Room temperature transmission Mössbauer spectra were obtained using a conventional constant acceleration spectrometer with a 25 mCi source of ^{57}Co in Rh matrix. Experimental spectra were fitted with TRANSMOS program [15], considering one or two histogram magnetic hyperfine-field distributions with linear correlation between the isomer shift and the magnetic field. The isomer shift values are given relative to room temperature α-Fe.

3. Results and discussion

Samples of $Fe_{72}B_{20}Si_4Nb_4$ metallic glass in as-cast state were examined by XRD, TEM and Mössbauer methods to check their amorphous state before annealing process.

The X-ray diffraction investigations revealed that the tested samples are amorphous. The diffraction patterns of tested ribbon samples have shown the broad diffraction halo characteristic for the amorphous structure (Fig. 1).

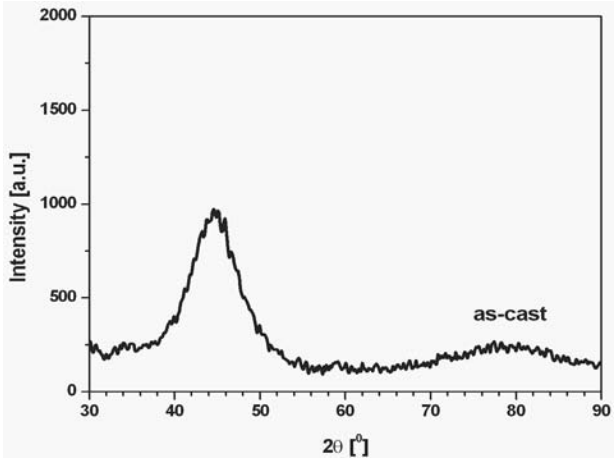

Fig. 1. X-ray diffraction pattern of $Fe_{72}B_{20}Si_4Nb_4$ metallic glass in as-cast state

TEM examination implied no crystal structure of studied material. Figure 2 shows the TEM micrograph including a structure image and a selected electron diffraction pattern with a halo rings caused by the amorphous structure.

Figure 3 shows transmission Mössbauer spectra measured at room temperature for the $Fe_{72}B_{20}Si_4Nb_4$ alloy in as-cast state. The spectrum exhibits the broad six-line pattern characteristic of ferromagnetic amorphous alloys.

In the hyperfine field distribution (Fig. 4) obtained from this spectrum one can distinguish components related to the regions with the different iron concentration.

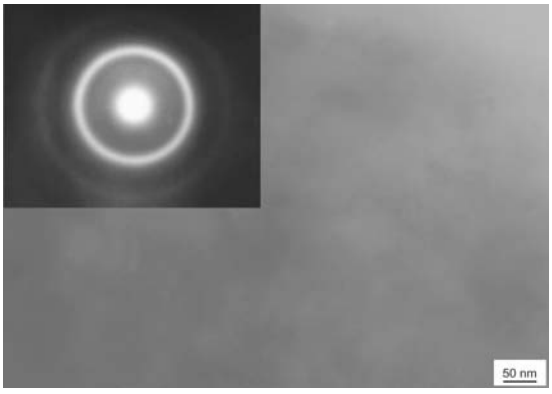

Fig. 2. Transmission electron micrograph and electron diffraction pattern of $Fe_{72}B_{20}Si_4Nb_4$ metallic glass in as-cast state

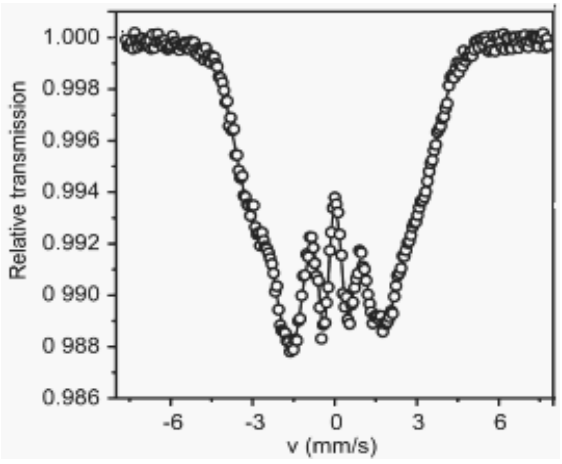

Fig. 3. Transmission Mössbauer spectra for $Fe_{72}B_{20}Si_4Nb_4$ metallic glass in as-cast state

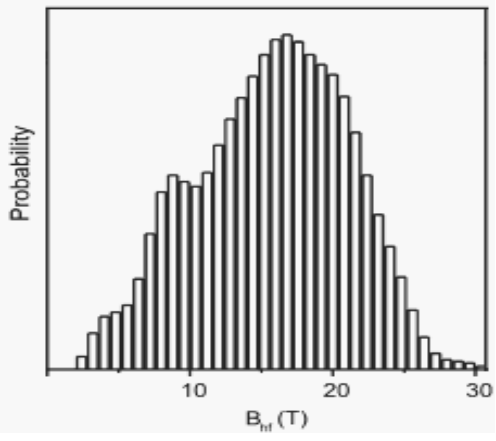

Fig. 4. Hyperfine field distribution for $Fe_{72}B_{20}Si_4Nb_4$ metallic glass in as-cast state

The DTA curves measured on amorphous samples in as-cast state for examined alloy composition are shown in Figure 5. Two crystallization effects (exothermic peaks) were observed for $Fe_{72}B_{20}Si_4Nb_4$ amorphous alloy. The first stage crystallization of studied glassy alloy includes onset crystallization temperature (T_{x1} = 842 K) and peak crystallization temperature (T_{p1} = 864 K). Analysis of the second crystallization effect allows to determine only peak crystallization temperature (T_{p2} = 892 K), as well.

The melting temperature (T_m) and liquidus temperature (T_l) assumed to be the onset and end temperature of the melting isotherm on the DTA curve is presented in Figure 6. Two endothermic peaks observed on DTA curve of master alloy of studied metallic glass allowed to determine the melting temperature (T_m), which has a value of 1363 K and liquidus temperature (T_l = 1560 K).

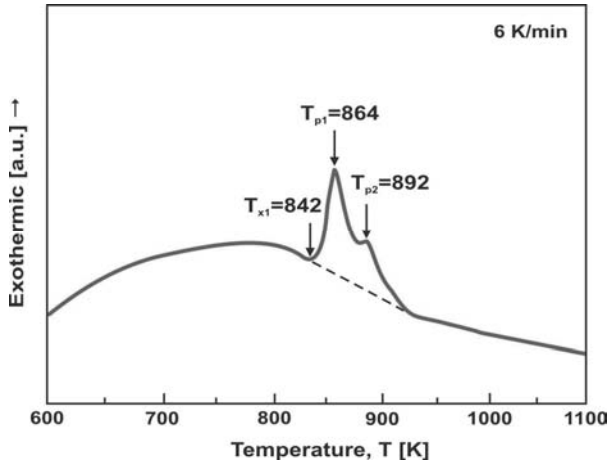

Fig. 5. DTA curve of $Fe_{72}B_{20}Si_4Nb_4$ glassy alloy in as-cast state

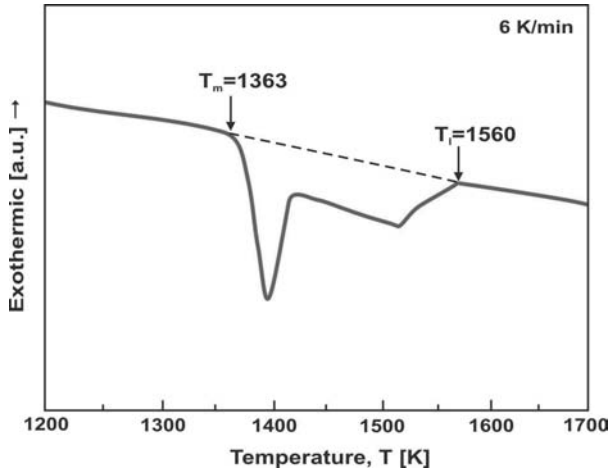

Fig. 6. DTA curve of $Fe_{72}B_{20}Si_4Nb_4$ alloy as master-alloy

Figure 7 shows X-ray diffraction patterns obtained for studied alloy after annealing at 373, 573 and 773 K for 1 hour. It is noticed, that annealing in studied temperature range does not lead to a formation of any crystallites detectable by X-ray diffraction and TEM techniques (Figs. 9 - 11).

Comparison of diffraction patterns of studied alloy after annealing from 373 K to 773 K shows the narrowing of diffraction lines and increase of their intensity. What is more, the TEM images reveal only a changing of contrast of amorphous phase.

These effects indicate that annealing process causes structural relaxation of tested amorphous materials, which leads to changes in their physical properties. These changes are probably due to atomic rearrangements that lead to changes in free volume [4].

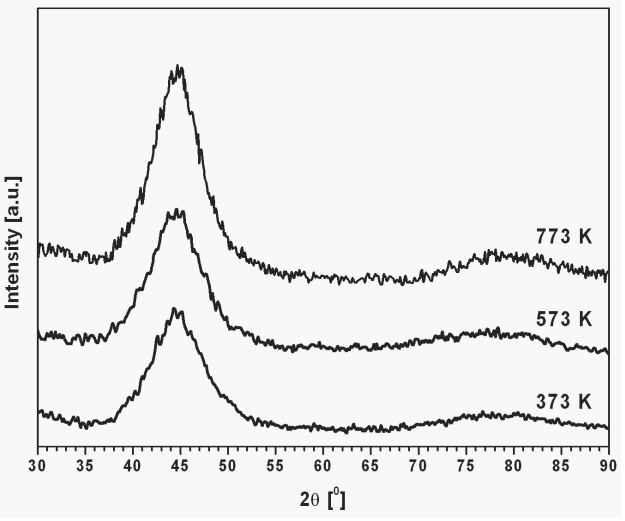

Fig. 7. X-ray diffraction patterns of $Fe_{72}B_{20}Si_4Nb_4$ alloy after annealing at 373, 573 and 773 K for 1 hour

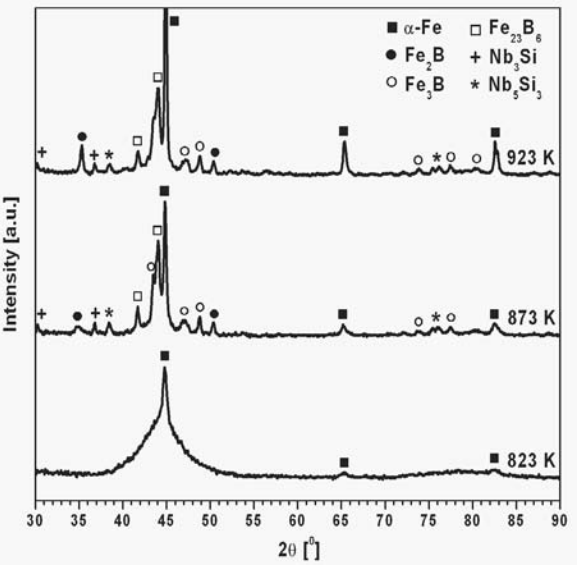

Fig. 8. X-ray diffraction patterns of $Fe_{72}B_{20}Si_4Nb_4$ alloy after annealing at 823, 873 and 923 K for 1 hour

Annealing at higher temperatures obviously causes formation of crystalline phases (Fig.8). Qualitative phase analysis from X-ray data enables the identification of α-Fe phase (823 K) and borides Fe_2B, Fe_3B and $Fe_{23}B_6$ (873 K and 923 K). Moreover, X-ray diffraction investigations allow to detection Nb_3Si and Nb_5Si_3 phases.

It could be noticed that the first stage of crystallization of studied corresponding to the partial crystallization of α-Fe phase was followed by the formation of iron borides.

Moreover, TEM images and electron diffraction patterns obtained for samples annealed at 823, 873 and 923 K confirmed a formation of crystalline phases (Fig.12 -14).

Figure 15 shows transmission Mössbauer spectra measured at room temperature for the $Fe_{72}B_{20}Si_4Nb_4$ alloy after annealing at 873 K for 1 hour.

The maxima of hyperfine field distribution for $Fe_{72}B_{20}Si_4Nb_4$ after annealing at 873 K for 1 hour (Fig.16) are respectively confirmed the presence of Fe-B environment, $Fe_{23}B_6$-type phase and α-Fe phase.

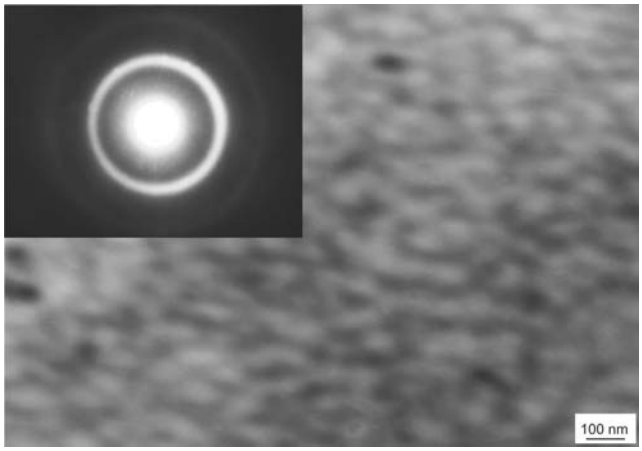

Fig. 11. Transmission electron micrograph and electron diffraction pattern of $Fe_{72}B_{20}Si_4Nb_4$ alloy after annealing at 773 K for 1 hour

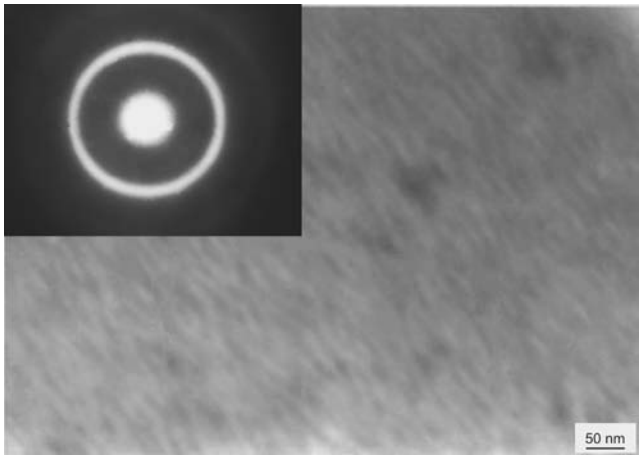

Fig. 9. Transmission electron micrograph and electron diffraction pattern of $Fe_{72}B_{20}Si_4Nb_4$ alloy after annealing at 373 K for 1 hour

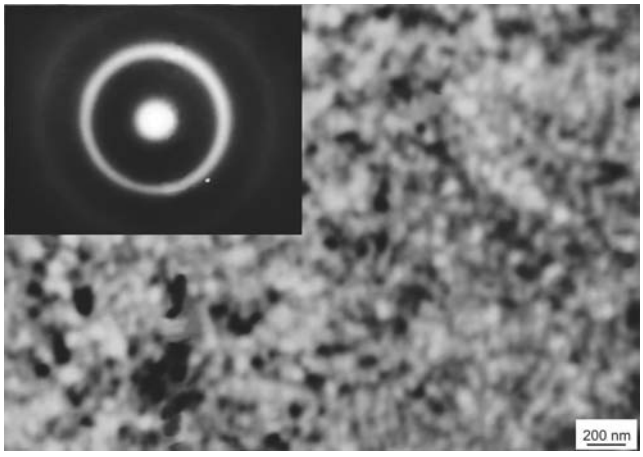

Fig. 12. Transmission electron micrograph and electron diffraction pattern of $Fe_{72}B_{20}Si_4Nb_4$ alloy after annealing at 823 K for 1 hour

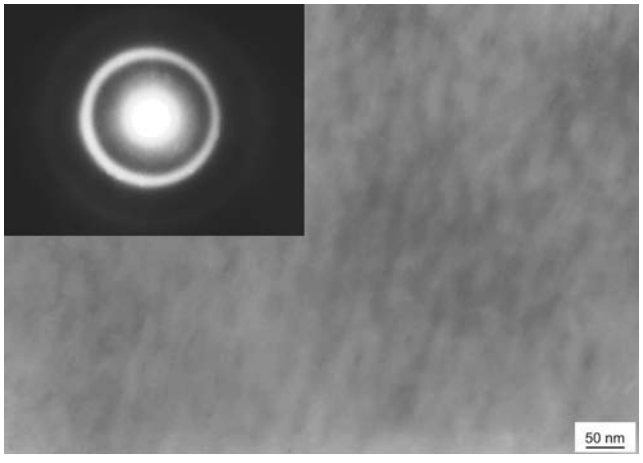

Fig. 10. Transmission electron micrograph and electron diffraction pattern of $Fe_{72}B_{20}Si_4Nb_4$ alloy after annealing at 573 K for 1 hour

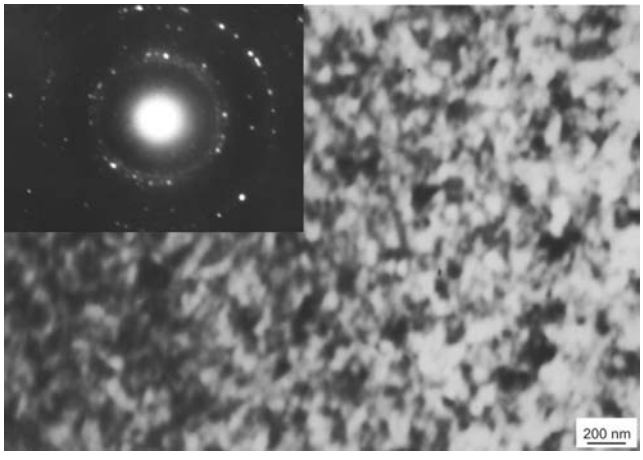

Fig. 13. Transmission electron micrograph and electron diffraction pattern of $Fe_{72}B_{20}Si_4Nb_4$ alloy after annealing at 873 K for 1 hour

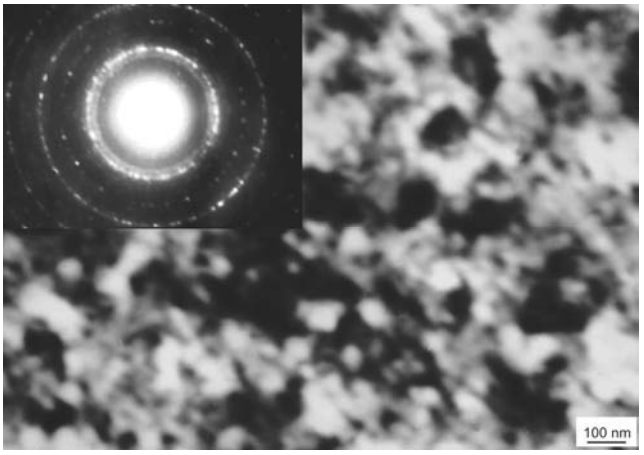

Fig. 14. Transmission electron micrograph and electron diffraction pattern of $Fe_{72}B_{20}Si_4Nb_4$ alloy after annealing at 923 K for 1 hour

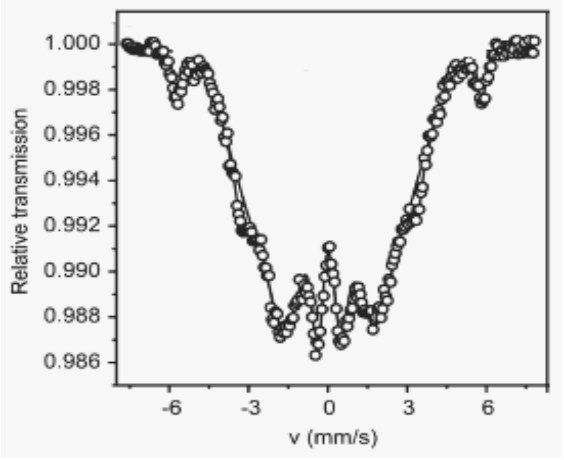

Fig. 15. Transmission Mössbauer spectra for $Fe_{72}B_{20}Si_4Nb_4$ after annealing at 873 K for 1 hour

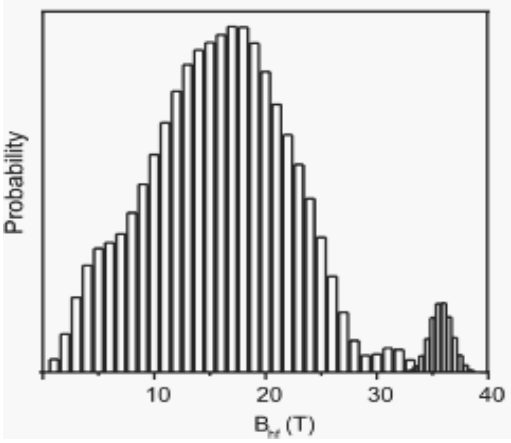

Fig. 16. Hyperfine field distribution for $Fe_{72}B_{20}Si_4Nb_4$ after annealing at 873 K for 1 hour

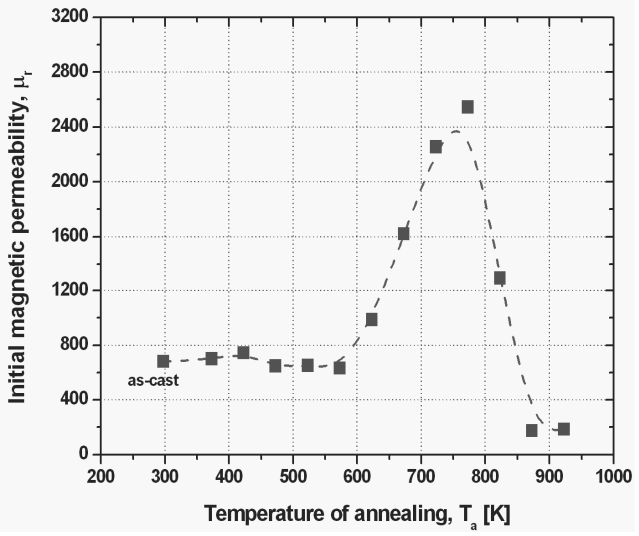

Fig. 17. Initial magnetic permeability of $Fe_{72}B_{20}Si_4Nb_4$ alloy determined at room temperature versus annealing temperature

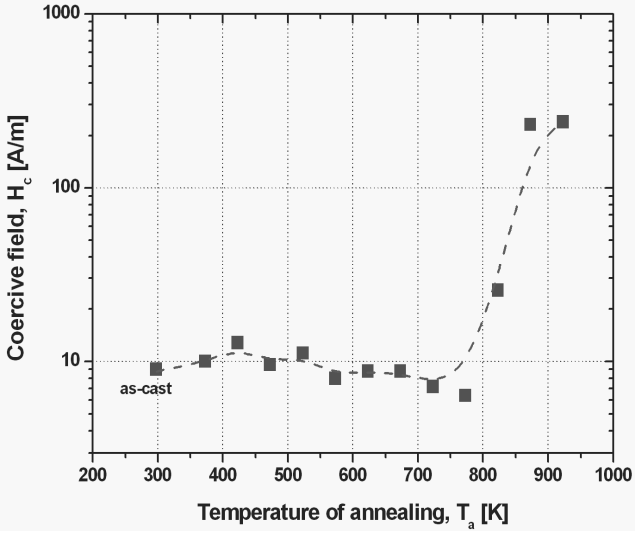

Fig. 18. Coercive field of $Fe_{72}B_{20}Si_4Nb_4$ alloy determined at room temperature versus annealing temperature

As is introduced in [16], these results indicate that, apart from the Fe-B type and α-Fe nanocrystals, a disordered type of environment, being respectively rich and poor in Nb, may exist in the nanocrystallized Fe-B-Si-Nb samples.

The initial magnetic permeability (μ_r) determined at room temperature versus annealing temperature (T_a) is shown in Figure 17. Initial magnetic permeability of studied material increase together with increasing of annealing temperature and reach a distinct maximum at 773 K. That temperature of annealing process corresponding to the maximum initial magnetic permeability (μ_{rmax} = 2500) and could be define as the optimization annealing temperature (T_{op}).

Moreover, Figure 18 presents the changes of coercive field plotted in logarithmic scale versus annealing temperature for examined alloy. Analysis of Figures 17 and 18 allows to concluded that a maximum of initial magnetic permeability is correlated with a minimum of coercive field (H_{cmin} = 6.4 A/m).

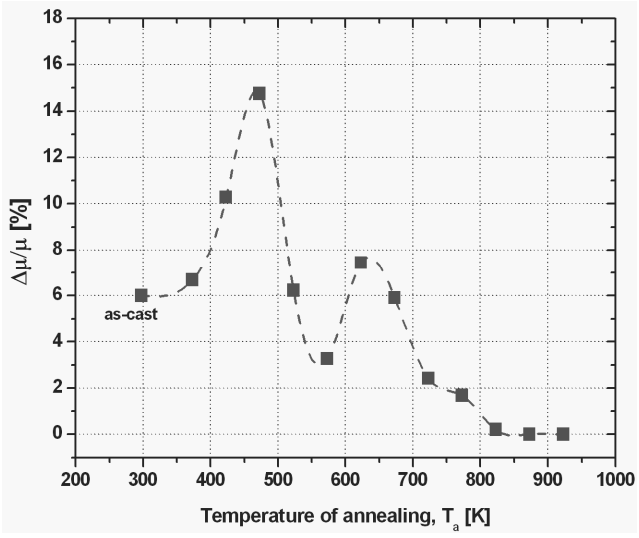

Fig. 19. Magnetic permeability relaxation of $Fe_{72}B_{20}Si_4Nb_4$ alloy determined at room temperature versus annealing temperature

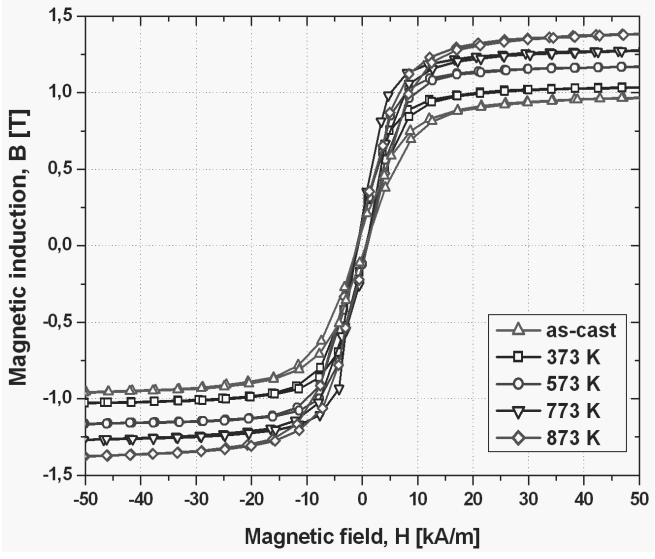

Fig. 20. Hysteresis loops of $Fe_{72}B_{20}Si_4Nb_4$ alloy in as-cast state and after annealing at 373, 573, 773 and 873 K

Figure 19 shows magnetic permeability relaxation (magnetic after-effects) in function of annealing temperature. The intensity of Δμ/μ is directly proportional to the concentration of defects in amorphous materials, i.e. microvoids concentration [2].

As could be observed from Figure 19, a value of Δμ/μ increases in the temperature range 373-473 K. That time instability of magnetic permeability is probably due to migration and coagulation of microvoids [12,13].

The successive increase of annealing temperature causes that Δμ/μ decreases. It is important that optimization annealing temperature (T_{op}) corresponds to a significant decrease of magnetic instability (Δμ/μ). This means that the optimization annealing reduces time instabilities of magnetic permeability.

The hysteresis loops obtained from VSM measurements allowed to determine a magnetic saturation induction (B_s) of tested samples after annealing at 373, 573, 773 and 873 K for one hour (Fig. 20).

As could be seen from Figure 20, a value of B_s increases during increasing of annealing temperature. The saturation induction of studied samples has a value of B_s = 1.03 T and 1.38 T for samples annealed at 373 K and 873 K, adequately. The magnetic saturation induction of samples annealed at optimization temperature (T_{op}) has a value of 1.27 T.

Table 2 also gives information about magnetic properties of studied alloy in state after optimization annealing temperature (T_{op}).

Table 2.
Magnetic properties of studied $Fe_{72}B_{20}Si_4Nb_4$ alloy at optimization annealing temperature (T_{op})

Glassy alloy	T_{op} [K]	B_s [T]	H_c [A/m]	μ_r	Δμ/μ [%]
$Fe_{72}B_{20}Si_4Nb_4$	773	1.27	6.4	2500	1.7

It is also shown that in studied alloy, the optimization effect (μ_r and H_c) takes place in amorphous phase. However, the obtained results confirmed that annealing at temperature T_{op} causes a real enhancement of soft magnetic properties in comparison with as-cast state of tested material.

4. Conclusions

The investigations performed on the samples of $Fe_{72}B_{20}Si_4Nb_4$ alloy after annealing process allowed to formulate the following statements:

- the X-ray diffraction, transmission electron microscopy and Mössbauer spectroscopy investigations revealed that the studied alloy in as-cast state is amorphous,
- a two stage crystallization process was observed for studied amorphous alloy,
- the annealing process from 373 to 773 K caused a structural relaxation of tested material, which leads to changes of its physical properties in relation to as-cast state,
- the annealing at higher temperatures (823 – 923 K) obviously caused a formation of crystalline phases,
- the Mössbauer spectroscopy confirmed the presence of a Fe-B environment, $Fe_{23}B_6$-type and α-Fe phases for sample after annealing at 873 K,
- initial magnetic permeability of studied material increased together with increasing of annealing temperature and reach a distinct maximum at 773 K,

- a maximum of initial magnetic permeability is correlated with a minimum of coercive field,
- optimization annealing temperature (T_{op}) corresponded to a significant decrease of magnetic instability ($\Delta\mu/\mu$),
- the annealing at temperature T_{op} caused a real improvement of soft magnetic properties in comparison with as-cast state of studied alloy.

Acknowledgements

The authors would like to thank Dr A. Zajączkowski, (Non-Ferrous Metals Institute, Gliwice), Mr W. Skowroński (Department of Electronics, AGH University of Science and Technology, Kraków) and Dr Z. Stokłosa (University of Silesia, Katowice) for a cooperation.

This work is supported by Polish Ministry of Science (grant N507 027 31/0661).

References

[1] T. Kulik, Nanocrystallization of metallic glasses, Journal of Non-Crystalline Solids 287 (2001) 145-161.
[2] J. Rasek, Some diffusion phenomena in crystalline and amorphous metals, Silesian University Press, Katowice, 2000 (in Polish).
[3] G. Badura, J. Rasek, Z. Stokłosa, P. Kwapuliński, G. Haneczok, J. Lelątko, L. Pająk, Soft magnetic properties enhancement effect and crystallization processes in $Fe_{78-x}Nb_xSi_{13}B_9$ (x = 0, 2, 4) amorphous alloys, Journal of Alloys and Compounds 436 (2007) 43-50.
[4] V.H. Hammond, M.D. Houtz, J.M. O'Reilly, Structural relaxation in a bulk metallic glass, Journal of Non-Crystalline Solids 325 (2003) 179-186.
[5] W.H. Wang, Crystallization of ZrTiCuNiBe bulk metallic glasses, Annales de Chimie Science des Materiaux 27/5 (2002) 99-105.
[6] R. Nowosielski, R. Babilas, Structure and magnetic properties of $Fe_{36}Co_{36}B_{19}Si_5Nb_4$ bulk metallic glasses, Journal of Achievements in Materials and Manufacturing Engineering 30/2 (2008) 135-140.
[7] R. Nowosielski, R. Babilas, P. Ochin, Z. Stokłosa, Thermal and magnetic properties of selected Fe-based metallic glasses, Archives of Materials Science and Engineering 30/1 (2008) 13-16.
[8] D. Szewieczek, J. Tyrlik-Held, S. Lesz, Structure and mechanical properties of amorphous $Fe_{84}Nb_7B_9$ alloy during crystallization, Journal of Achievements in Materials and Manufacturing Engineering 24/1 (2007) 87-90.
[9] D. Szewieczek, T. Raszka, J. Olszewski, Optimisation the magnetic properties of the $(Fe_{1-x}Co_x)_{73.5}Cu_1Nb_3Si_{13.5}B_9$ (x=10; 30; 40) alloys, Journal of Achievements in Materials and Manufacturing Engineering 20 (2007) 31-36.
[10] S. Lesz, D. Szewieczek, J.E. Frąckowiak, Structure and magnetic properties of amorphous and nanocrystalline $Fe_{85.4}Hf_{1.4}B_{13.2}$ alloy, Journal of Achievements in Materials and Manufacturing Engineering 19/1 (2006) 29-34.
[11] R. Nowosielski, R. Babilas, G. Dercz, L. Pająk, W. Skowroński, Microstructure and magnetic properties of $BaFe_{12}O_{19}$ powder, Journal of Achievements in Materials and Manufacturing Engineering 27/1 (2008) 51-54.
[12] P. Kwapuliński, J. Rasek, Z. Stokłosa, G. Badura, B. Kostrubiec, G. Haneczok, Magnetic and mechanical properties in FeXSiB (X=Cu, Zr, Co) amorphous alloys, Archives of Materials Science and Engineering 31/1 (2008) 25-28.
[13] P. Kwapuliński, J. Rasek, Z. Stokłosa, G. Haneczok, Magnetic properties of $Fe_{74}Cu_1Cr_xZr_{3-x}Si_{13}B_9$ amorphous alloys, Journal of Magnetism and Magnetic Materials 254-255 (2003) 413-415.
[14] J. Wrona, T. Stobiecki, M. Czapkiewicz, R. Rak, T. Ślęzak, J. Korecki, C.G. Kim, R-VSM and MOKE magnetometers for nanostructures, Journal of Magnetism and Magnetic Materials 272-276 (2004) 2294-2295.
[15] P. Gorria, J.S. Garitaonandia, J.M. Barandiarán, Structural and magnetic changes in FeNbCuSiB amorphous alloys during the crystallization process, Journal of Physics: Condensed Matter 8 (1996) 5925-5939.
[16] J. Torrens-Serra, P. Bruna, J. Rodríguez-Viejo, T. Pradell, M.T. Clavaguera-Mora, Study of crystallization process of $Fe_{65}Nb_{10}B_{25}$ and $Fe_{70}Nb_{10}B_{20}$ glassy metals, Reviews on Advanced Materials Sciences 18 (2008) 464-468.